Effects of body mass on microstructural features of the osteochondral unit

A comparative analysis of 37 mammalian species

Mancini, I. A.D.; Rieppo, L.; Pouran, B.; Afara, I. O.; Braganca, F. M.Serra; van Rijen, M. H.P.; Kik, M.; Weinans, H.; Toyras, J.; van Weeren, P. R.

DOI
10.1016/j.bone.2019.07.001

Publication date
2019

Document Version
Final published version

Published in
Bone

Bone 127 (2019) 664–673

Contents lists available at ScienceDirect

Bone

journal homepage: www.elsevier.com/locate/bone

Full Length Article

Effects of body mass on microstructural features of the osteochondral unit: A comparative analysis of 37 mammalian species

I.A.D. Mancini[a,b], L. Rieppo[c], B. Pouran[b,d,e], I.O. Afara[f], F.M. Serra Braganca[a], M.H.P. van Rijen[b,d], M. Kik[g], H. Weinans[b,d,e], J. Toyras[f,h,i], P.R. van Weeren[a,b], J. Malda[a,b,d,*]

[a] Department of Equine Sciences, Faculty of Veterinary Medicine, Utrecht University, the Netherlands
[b] Regenerative Medicine Utrecht, Utrecht University, Utrecht, the Netherlands
[c] Research Unit of Medical Imaging, Physics and Technology, Faculty of Medicine, University of Oulu, Oulu, Finland
[d] Department of Orthopedics, University Medical Centre Utrecht, Utrecht, the Netherlands
[e] Department of Biomechanical Engineering, TU, Delft, the Netherlands
[f] Department of Applied Physics, University of Eastern Finland, Kuopio, Finland
[g] Department of Pathobiology, Faculty of Veterinary Medicine, Utrecht University, the Netherlands
[h] Diagnostic Imaging Centre, Kuopio University Hospital, Kuopio, Finland
[i] School of Information Technology and Electrical Engineering, The University of Queensland, Brisbane, Australia

ARTICLE INFO

Keywords:
Osteochondral unit
Trabecular bone
Subchondral bone
Cartilage
Osteochondral comparative analysis
Scaling

ABSTRACT

Since Galileo's days the effect of size on the anatomical characteristics of the structural elements of the body has been a subject of interest. However, the effects of scaling at tissue level have received little interest and virtually no data exist on the subject with respect to the osteochondral unit in the joint, despite this being one of the most lesion-prone and clinically relevant parts of the musculoskeletal system.

Imaging techniques, including Fourier transform infrared imaging, polarized light microscopy and micro computed tomography, were combined to study the response to increasing body mass of the osteochondral unit. We analyzed the effect of scaling on structural characteristics of articular cartilage, subchondral plate and the supporting trabecular bone, across a wide range of mammals at microscopic level.

We demonstrated that, while total cartilage thickness scales to body mass in a negative allometric fashion, thickness of different cartilage layers did not. Cartilage tissue layers were found to adapt to increasing loads principally in the deep zone with the superficial layers becoming relatively thinner. Subchondral plate thickness was found to have no correlation to body mass, nor did bone volume fraction. The underlying trabecular bone was found to have thicker trabeculae ($r = 0.75$, $p < 0.001$), as expected since this structure carries most loads and plays a role in force mitigation.

The results of this study suggest that the osteochondral tissue structure has remained remarkably preserved across mammalian species during evolution, and that in particular, the trabecular bone carries the adaptation to the increasing body mass.

1. Introduction

Almost 400 years ago, after visiting Venice's Arsenal, Galileo laid the foundations to modern deformable body mechanics, by starting a discussion about scaling [1]. He took inspiration from shipbuilding and wondered how structural components would scale in bigger ships to avoid collapsing under excessive weight. This led to the formulation of the Square-Cube law that Galileo formulated as “the ratio of two volumes is greater than the ratio of their surfaces” [1]. In other words, when an object undergoes a proportional increase in size, its surface area is proportional to the square of the multiplier, while its volume is proportional to the cube of the multiplier. In addition, it also means that the stress on a larger cube is greater than the stress on a smaller cube due to its own weight [2]. Later, in the Discourses and

Abbreviations: BM, Body mass; PGs, Proteoglycans; CCZ, Calcified cartilage zone; ROI, Region of interest; FTIRI, Fourier transform infrared imaging; PLM, Polarized light microscopy; Micro-CT, Micro computed tomography; Sc.Th, Subchondral plate thickness; Sc.BV/TV, Subchondral bone volume fraction; Tb.Th, Trabecular thickness; Tb.BV/TV, Trabecular bone volume fraction

* Corresponding author at: Department of Equine Sciences, Faculty of Veterinary Medicine, Utrecht University, the Netherlands.
E-mail address: j.malda@uu.nl (J. Malda).

https://doi.org/10.1016/j.bone.2019.07.001
Received 15 February 2019; Received in revised form 28 June 2019; Accepted 2 July 2019
Available online 03 July 2019
8756-3282/

Mathematical Demonstrations Relating to Two New Sciences, Galileo applied the law to living beings and deduced that animals could not be simply scaled up, or their bones would break under excessive weight [1]. Since then, macroscopic scaling of limbs and their components has been discussed extensively in literature [3–6]. Nevertheless, investigations on the microscopic level have been limited [7–10]. In particular, the adaptations to loading of the ensemble of the articular components (*i.e.* subchondral bone, cartilage and their interface) at microscopic level have never been analyzed in a comparative fashion across a large range of species.

The general structure and organization of diarthrodial joints is similar in all mammalian species. The function of these diarthrodial joints is both to minimize friction of the articulating bony components of the skeleton and to accommodate and mitigate the substantial biomechanical forces that are generated by locomotion. Hence, joint function requires its elements to provide excellent lubrication between articulating surfaces, allow force transmission and absorption, to mitigate the effects of acceleration, vibrations and peak forces generated by locomotion. To accomplish these tasks, joint components work in synergy and should be considered as a unit [11,12], composed of articular cartilage, the subchondral bone plate and trabecular bone rather than as individual components.

Basic biochemistry, biomechanics and morphological characteristics of the major components of diarthrodial joints (*i.e.* hyaline articular cartilage and bone) have been studied frequently in relation to pathological changes and effectiveness of different treatments [12–15]. These studies, however, are usually focused on humans and animal species that are of interest as models for orthopedic research in a translational sense [15,16]. In nature, the spectrum of sizes and body weights in mammals is much wider than in the few species used as animal models for musculo-skeletal diseases [7,17]. We have previously shown in a study over a wide range of species that articular width in the stifle (knee) joint scales isometrically with body mass [7]; this isometric relation can be mathematically described as $y = bx^{a}$, with $a = 0.33$ [7]. If we assume that joint form is not essentially influenced by size, joint surface will do the same [18]. If then the microscopic configuration of the osteochondral unit would remain the same, the stress in the unit would increase linearly with weight given the Square-Cube law. Both articular cartilage and bone increase in size with body mass, and isolated studies on these two tissues have shown that they do not scale isometrically, but have a negative allometric relationship with increasing body mass [7–9] and therefore do not fully compensate for increasing body mass. In theory, an increase in loading can also be compensated for by changes in composition of the constituting elements of the osteochondral unit (that would possibly influence strength of the structure). However, previous research comparing articular cartilage biochemical composition across a variety of mammalian species covering a range of body masses revealed that gross biochemical composition was constant [7]. The composition and structure of articular cartilage, however, does change with depth, so that three layers (superficial, middle and deep) can be identified, based on compositional characteristics like proteoglycans and collagen content, and structural characteristics like collagen orientation. In this last case, fibrils are oriented parallel to the articular surface in the superficial zones, and transition through a random orientation to the deep zone in which they are oriented perpendicular to the subchondral bone [19].

The current study aims to comprehensively investigate the microstructural and compositional features of the osteochondral unit (across a wide range of terrestrial mammals) and their relationship to each other and to body mass (BM). This will reveal where the adaptations to increasing loads (and BM) [20] reside and will determine which microscopic features follow isometric scaling and which do not.

It was hypothesized that in articular cartilage all layers would scale with negative allometry, as found earlier for total thickness [7], and that increased load would be accommodated by either structural adaptations in the subchondral plate or the trabecular subchondral bone, or by adaptations of the components in one or more of these layers.

2. Materials and methods

To investigate spatial biochemical composition of single layers of cartilage, *Fourier-Transform Infrared Imaging* (FTIRI) [21–23] was employed, allowing to determine relative content of proteoglycans (PG) and collagen by measuring absorption of specific peaks [24]. To evaluate the orientation and distribution of the cartilaginous collagen network, *Polarized Light Microscopy* (PLM) was chosen for its capacity to visualize the orientation of anisotropic materials [25–27]. Finally, for the detailed analysis of the microstructural features of the subchondral and trabecular bone, *micro computed tomography* (micro-CT) was selected for the accurate measurement of micron-sized structures that constitute the bony tissue [28,29].

2.1. Collection of materials and tissue harvest

Osteochondral tissue cylinders of 6 mm in diameter were harvested post-mortem from the weight bearing central area of the medial femoral condyles of adult animals sent for autopsy to the Department of Pathobiology, Faculty of Veterinary Medicine, Utrecht University, The Netherlands. Animal species, age and body mass were recorded, and macroscopic pictures of the joints were taken. Joints demonstrating macroscopic or microscopic signs of cartilage degeneration were excluded; animals displaying signs of incomplete endochondral ossification were identified as immature and excluded as well. Human tissue samples were obtained from the Department of Pathology, University Medical Center Utrecht, The Netherlands, with approval of the local ethical committee, in line with the Dutch code of conduct for “Proper Secondary Use of Human Tissue”.

In total 82 tissue samples (38 for histological analysis, 44 for micro-CT) were harvested from mammals belonging to 37 different species; of 38 histological samples, 5 samples could not be measured with PLM and 7 samples could not be measured with FTIRI (Table 1). Due to limited amount of tissue available, measurement with micro-CT of trabecular parameters of 4 of the 44 samples (Table 1) was not possible. Samples for histology were fixed in formalin 4%, while samples for micro-CT analysis were stored in 70% ethanol; all samples were stored at room temperature until further use.

2.2. Histological preparation and analysis

Samples were decalcified using Luthra solution (3.2% 11M HCl, 10% formic acid in distilled water), dehydrated, cleared in xylene, embedded in paraffin and cut to yield 5 μm sections. Sections were stained with fast green and Safranin-O for measurements of cartilage thickness (distance from the surface to the interface with the subchondral bone), and of the calcified cartilage zone (from tidemark to bone surface). Digital images were analyzed using CellˆF software (Olympus, USA). Average thickness of cartilage and calcified cartilage zone (CCZ) for each sample was determined by averaging 4 measurements per image taken from different locations of the section.

2.3. Fourier-transform infrared imaging (FTIRI) and polarized light microscopy (PLM)

Unstained histological sections were inserted in a controlled atmosphere chamber without humidity and specific regions of interest (ROIs) of the full thickness of the cartilaginous tissue (Fig. 1A) were measured using a Fourier transform infrared imaging system (PerkinElmer Spectrum Spotlight 300-system). The absorption spectrum of a pixel ($25 \times 25\ \mu m^2$) was translated to relative values (Fig. 1B). Collagen content was estimated with amide I (1585–1720 cm^{-1}) absorption and PGs with absorption at carbohydrate region 984–1140 cm^{-1}

Table 1
List of species included in the study. In total 82 tissue samples (38 for histological analysis, 44 for micro-CT) were harvested from mammals belonging to 37 different species; of the 38 histological samples, 33 were measured with PLM and 31 were measured with FTIRI. Forty-four samples were measured with micro-CT, however due to limited amount of tissue available, in 4 cases trabecular parameters could not be measured (indicated in brackets are the samples measured for trabecular parameters).

	Species	Average body mass (kg)	PLM (n)	FTIRI (n)	Micro-CT (n)
1	Mouse (*Mus musculus*)	0.03			3
2	Rat (*Rattus* sp.)	0.3	2	2	3
3	Ferret (*Mustela putorius furo*)	2	1	1	
4	Hare (*Lepus* sp.)	3.15	2	2	
5	South American coati (*Nasua nasua*)	3			1
6	Linnaeus's two-toed sloth (*Choloepus didactylus*)	6.5	1	1	
7	Barbary macaque (*Macaca sylvanus*)	8.5			2
8	European Badger (*Meles meles*)	10	1	1	
9	Kirk's dik-dik (*Madoqua kirkii*)	10	1	1	
10	Tammar wallaby (*Macropus eugenii*)	12.5	2	2	2
11	Indian crested porcupine (*Hystrix indica*)	16	1	1	
12	Hamadryas baboon (*Papio hamadryas*)	17			2
13	Roe deer (*Capreolus capreolus*)	17	2	2	3(2)
14	Thomson's gazelle (*Eudorcas thomsonii*)	18	3	3	3(2)
15	Dwarf goat (*Capra aegragus hircus*)	28	1	1	1
16	Cheetah (*Acinonyx jubatus*)	39			3
17	Impala (*Aepyceros melampus*)	41	1	1	2
18	Red kangaroo (*Macropus rufus*)	55	2	2	2
19	Human (*Homo sapiens*)	65	1	1	
20	Fallow deer (*Dama dama*)	70	1	1	1
21	Gorilla (*Gorilla gorilla)*	80			1
22	Siberian tiger (*Panthera tigris*)	80			1
23	Reindeer (*Rangifer tarandus*)	125	1	1	
24	Lion (*Panthera leo*)	148			1
25	Greater Kudu (*Tragelaphus strepsiceros*)	150			
26	Llama (*Lama glama*)	160	1	1	
27	Polar bear (*Ursus maritimus*)	175			1
28	South American tapir (*Tapirus terrestris*)	250			1
29	Elk (*Alces alces*)	343	1	1	1
30	Watussi (*Bos taurus taurus watussi*)	350	1		
31	Dairy cow (*Bos taurus*)	450	1	1	
32	Rothschild's giraffe (*Giraffa camelopardalis*)	470	1	1	2(1)
33a	Shetland pony (*Equus ferus caballus*)	150	1	1	
33b	Horse (*Equus ferus caballus*)	550	3	2	3(2)
34	Banteng (*Bos javanicus*)	600	1	1	1
35	White rhinoceros (*Ceratotherium simum*)	1400			1
36	Asian elephant (*Elephas maximus*)	3350			2
37	African elephant (*Loxodonta africana*)	4000			1
	Total		33	31	44(40)

[23,24] (Fig. 1C). The values obtained for each pixel within the ROI constituted a matrix with information on PG and collagen contents, which was subsequently used for detailed analysis of the zonal structure of cartilage tissue (Fig. 1B).

Collagen fiber orientation was visualized using PLM, and used for the classification of the superficial, middle and deep layer of cartilage [25,30] (Fig. 2). An Abrio PLM system (Cri Inc., Woburn, MA, USA) mounted on a light microscope (Nikon Diaphot TMD, Nikon Inc.) was used for the PLM measurements. The area with the minimum birefringence value was assumed to be the border between the superficial and the middle zones, whereas the deep zone was considered to begin when the orientation angle values reached a plateau (typically close to 90 degrees with respect to cartilage surface) [31,32] (Fig. 2B, E). Birefringence depends strongly on the anisotropy of collagen fibrils: birefringence is high when fibrils are aligned to same direction with each other, and, in contrast, low when fibrils are randomly oriented. Therefore, high birefringence is seen in superficial and deep zones of cartilage, but low birefringence is observed in the middle zone where the fibrils are randomly oriented. Based on this, the minimum birefringence value is assumed to represent the border between the superficial and middle zones [32] (Fig. 2C, F).

The combination of this information with the quantitative data contained in the matrix obtained with FTIRI allowed for relative quantification of proteoglycans and collagen in selected regions, and layer by layer. The PLM allowed also quantifying of individual cartilage layer thickness (superficial, middle and deep).

2.4. Micro-CT

Micro Computed Tomography (micro-CT) images of the osteochondral cores were obtained with a micro-CT scanner (Quantum FX, Perkin Elmer, USA, voxel size = 20 μm^3). The automatically reconstructed micro-CT images were subsequently converted to series of 2D TIFF images and were binarized using local thresholding (Bernsen technique). BoneJ software [33] was used to determine thickness and bone volume fraction (Sc.BV/TV) of the subchondral plate/calcified cartilage with manual selection of the ROI, which started from the beginning of mineralized tissue under cartilage, and continued to the beginning of trabecular bone (Fig. 3A); trabecular thickness (Tb.Th) and bone volume fraction (Tb.BV/TV) of the underlying trabecular bone were also determined with the same methodology. To obtain true subchondral plate thickness, CCZ thickness was measured by light microscopy (Fig. 3B), and its value was subtracted from the CT measurements to obtain real subchondral plate thickness (Sc.Th, Fig. 3C).

2.5. Statistics

Initial statistical analysis was performed with R software 3.5.0 [34], to obtain a correlation matrix with Pearson coefficients [35,36]. A weighted correlation of the parameters showing possible dependencies

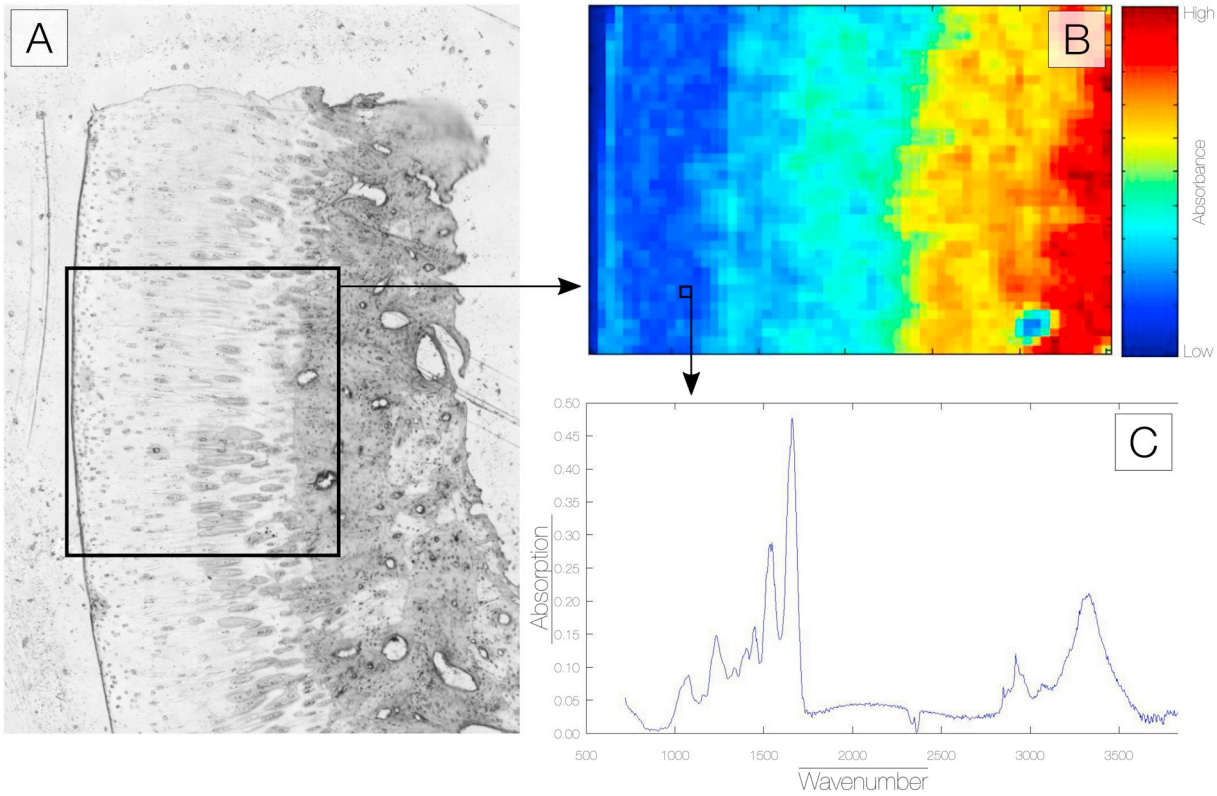

Fig. 1. Fourier transform infrared imaging (FTIRI) methodology. ROIs were selected using as reference the margin of cartilage interfacing with the synovial joint space, and the interface with the subchondral bone plate (A). The ROI was divided in pixels of 25 × 25 μm^2 (B, black square), and infrared absorption spectra were recorded for each pixel (C). The absorption for specific intervals was calculated to obtain relative contents of collagen and proteoglycans. Collagen content was estimated with amide I (1585–1720 cm^{-1}) absorption and PGs with absorption at carbohydrate region (984–1140 cm^{-1}). The values obtained for each pixel within the ROI constituted a matrix with information on PG and collagen contents, which was subsequently used for detailed analysis of the zonal structure of cartilage tissue.

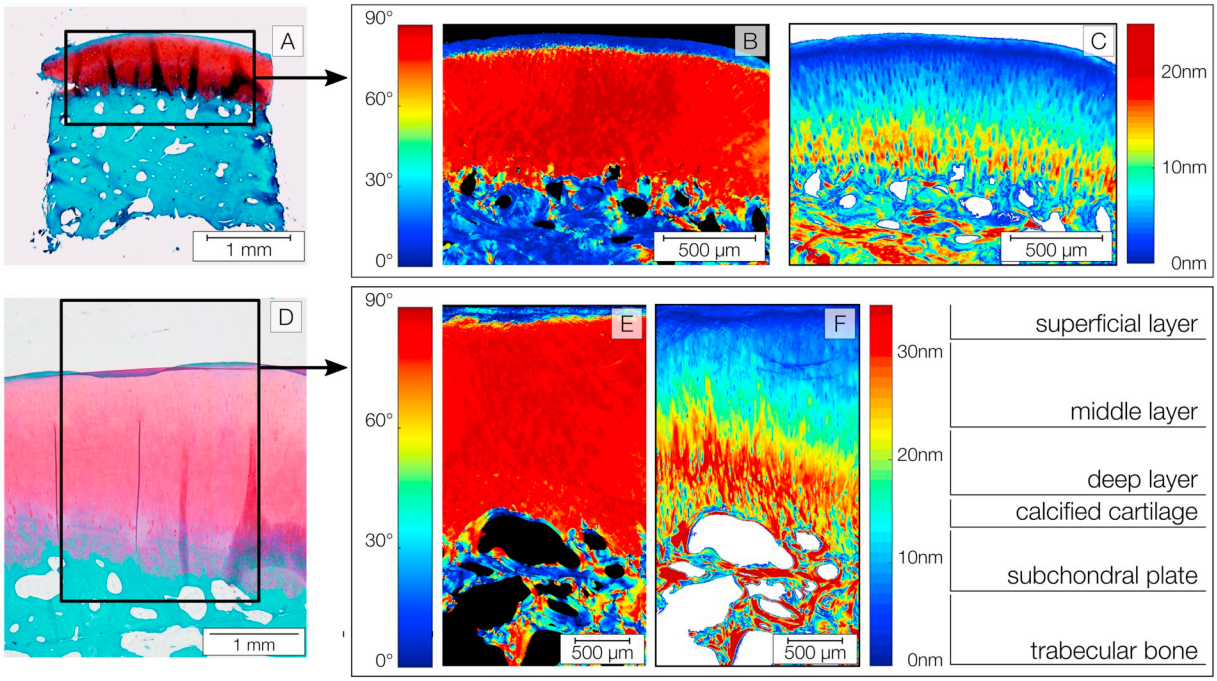

Fig. 2. Osteochondral microscopic images of Thompson's gazelle (20 kg, Top) and Giraffe (609.5 kg, bottom). Left images show sections stained for glycosaminoglycans with safranin-O (A, C). Centre images are collagen orientation maps obtained using polarized light microscopy images (PLM) (B, D). Blue colour indicates that fibers are parallel to the surface, while red indicates fibers having perpendicular orientation. The use of PLM allows determination of collagen fibers orientation, and consequently of the transition from superficial, to middle to deep layer of cartilage. Right images are retardance images obtained with PLM (birefrincence maps, C, F). (For interpretation of the references to colour in this figure legend, the reader is referred to the web version of this article.)

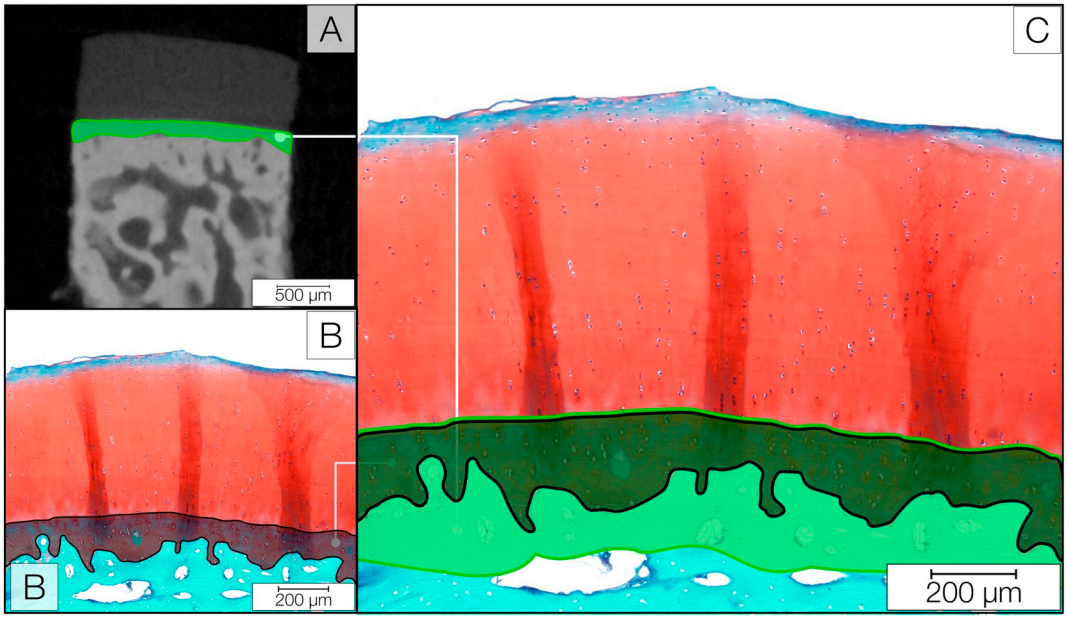

Fig. 3. Micro-computed tomography (micro-CT) images of the osteochondral cores were obtained with a micro-CT scanner (Quantum FX, Perkin Elmer, USA, resolution 20 µm). ROIs were selected manually (A, green), and used to determine subchondral plate thickness with BoneJ software. As micro-CT cannot discriminate between calcified cartilage and subchondral bone, CCZ thickness was measured using light microscopy (B, black), and its value was subtracted from the CT measurements (C, green selection) to obtain Sc Th. (For interpretation of the references to colour in this figure legend, the reader is referred to the web version of this article.)

was performed using the R-package "wCorr" version 1.9.1. Comparisons between multiple groups were performed using a one-way ANOVA combined with post-hoc *t*-tests with Bonferroni correction. Statistical comparison of the obtained power coefficients with the theoretical coefficient of 0.33 (isometric scaling) was performed using a one-sample *t*-test. Limit of statistical significance was set at $p < 0.05$.

3. Results

3.1. Depth-wise architecture of articular cartilage

Thickness of the cartilage layer (calcified plus non-calcified) varied widely between species, ranging from 64.6 µm in the mouse to 3.25 mm in the African elephant. Calcified cartilage thickness ranged from 46.4 µm in the mouse to 310 µm in the African elephant. Total cartilage thickness correlated with body mass (BM) with a negative allometric relationship ($R^2 = 0.83$, $\alpha = 0.29$, Fig. S1), in line with previous findings of Malda et al. [7].

Layer thickness of each layer was normalized to superficial layer thickness to show how layers relate to each other (Fig. 4A). Relative layer thickness was expressed for each layer as a percentage of total thickness, and correlated to BM. The relative thickness of the deep zone of the articular cartilage showed an increasing trend in relation to BM, whereas the relative thicknesses of both the superficial and the middle zone showed a tendency to decrease proportionally in relation to body size (Fig. 4B). Absolute values for the thickness of the single cartilage layers varied allometrically with BM (superficial layer, $r = 0.60$, $p < 0.05$ $\alpha = 0.17$, Fig. 4C) (middle layer, $r = 0.65$, $p < 0.05$ $\alpha = 0.19$, Fig. 4D) and isometrically with BM for the deep layer ($r = 0.82$, $p < 0.05$ $\alpha = 0.33$, Fig. 4E).

Combination of FTIRI and PLM techniques allowed for relative quantification and comparison (dimensionless numbers) of spatial collagen and PG content across species. Relative total collagen and PG content, when measured over the total thickness of the cartilage, showed no dependency to BM (Fig. 5A, B), with a small variation in composition across all species when considering content on the whole thickness of the tissue. Layer-by-layer analysis (superficial, middle, deep) showed this was true in all cartilage layers for both collagen and proteoglycans (Fig. 5C, D). Normalizing the contents of collagen and PG to superficial layer content, deep layer content was highest, and superficial layer was lowest for both collagen and PG and showed significant differences between layers (Fig. 5E, F, $p < 0.05$).

3.2. Subchondral and trabecular bone structure

Subchondral bone volume fraction (Sc.BV/TV) showed a positive correlation to Sc.Th ($r = 0.75$, $p < 0.001$). No correlation was found between Sc.BV/TV and Sc.Th to BM (Fig. 6A). The thickness of the subchondral plate ranged from 67.25 µm in the mouse to 1.13 mm in the horse. Mean subchondral plate thickness (Sc.Th, Table S1) was highest in the equine species (901 ± 344 µm, $n = 3$), while in the rats it was 205 ± 24 µm ($n = 3$) (Fig. 6B), and in the elephants the thickness was 149 ± 59 µm ($n = 3$) (Fig. 6C). Sc.BV/TV ranged from 95.8% ± 1.86% in mice ($n = 3$) to 99.7% ± 0.15% in horses ($n = 3$).

Trabecular thickness (Tb.Th) correlated with BM in a negative allometric relationship ($r = 0.72$, $p < 0.001$, $a = 0.14$, Fig. 6D). Trabecular thickness (Tb.Th, Table S1) ranged from 69.22 ± 2.87 µm ($n = 3$) in the mouse, 139.6 ± 9.13 µm ($n = 3$) in the rats (Fig. 6E), to 489.37 ± 79.86 µm ($n = 2$) in the elephants (Fig. 6F). Trabecular bone volume fraction (Tb.BV/TV) showed a positive correlation with BM ($r = 0.36$, $p < 0.05$), and trabecular thickness and trabecular BV/TV also showed a strong correlation between each other ($r = 0.67$, $p < 0.001$).

An analysis of the log ratio of thickness of cartilage, subchondral bone and trabecular bone, was performed to visualize differences between animals at the extremities of our BM range (*i.e.* belonging to the Muridae family and to the Elephantidae family), however statistical analysis revealed no significant differences (Fig. 7).

4. Discussion

A comprehensive analysis of how the osteochondral unit changes with body mass was performed using a combination of different techniques for measuring the microstructural features. Overall articular

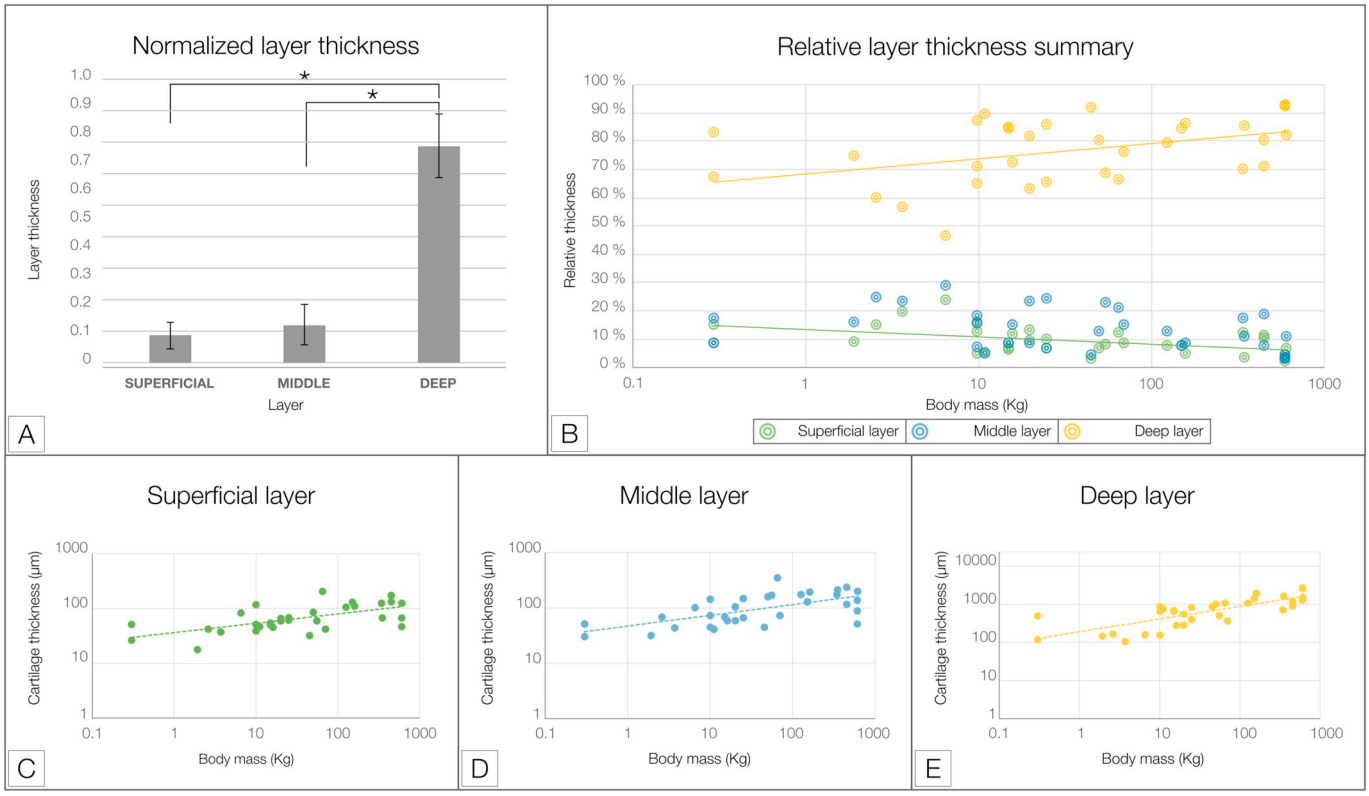

Fig. 4. Summary of cartilage scaling along body mass. Thickness of each layer was normalized to total layer thickness to show layers' relation to each other (A), showing significant differences between layers ($*p < 0.05$). Relative layer thickness (% of total thickness) was represented for each layer and correlated to BM (B). Relative deep zone thickness (yellow) showed an increasing trend in relation to BM whereas relative superficial (green) and middle (blue) zone thickness showed a tendency to decrease along increasing BM (B). Absolute values for the thickness of the single cartilage layers varied allometrically with BM (superficial layer, $r = 0.60, p < 0{,}05\ \alpha = 0.17$, C) (middle layer, $r = 0.65, p < 0{,}05\ \alpha = 0.19$, D) and isometrically with BM for the deep layer ($r = 0.82, p < 0{,}05\ \alpha = 0.33$, E). (For interpretation of the references to colour in this figure legend, the reader is referred to the web version of this article.)

cartilage thickness scaled in a negative allometric fashion, confirming earlier findings [7].

The current study showed that, contrary to our first hypothesis, both superficial and intermediate layers become relatively thinner single layer, whereas the deep layer seems to scale isometrically. The explanation may be that the deep zone is richest in PGs and hence thought to be primary responsible of transmission of load to the underlying bone [37–39], and therefore may need to scale accordingly to BM. This would also be in line with the role that is attributed to the superficial layer [40,41], which is thought to have a major role in the homogeneous distribution of the impact forces and loads away from directly-loaded regions [42,43], more than in load attenuation and with the fact that in physics, as one scales down, forces like viscous drag become more important than weight [1,44].

The biochemical composition of articular cartilage was remarkably consistent across species in both absolute and relative terms. This suggests that evolutionary pressure has led to the best possible combination of PG and collagen to effectuate the duty of shock-absorption and transfer of forces to the subchondral and trabecular bone in terrestrial locomotion. The normalization of content to total layer thickness confirmed layer dependency highlighting significant difference between the deep layer and the superficial and middle layers ($*p < 0.05$), as was expected from previous studies on selected species [45]. However, as remarkable as it seems that there are no substantial variations in the major structural components of cartilage from mouse to elephant, there may be some in characteristics of those components that were not specifically measured, such as the post-translational modifications of collagen of which cross-links are the most likely candidates.

Benninghoff (1925) first described the arching structure formed by the collagen fibers of articular cartilage that run from their anchoring site in the calcified zone first through the deep zone, directed perpendicularly to the subchondral plate, to then describe an arch at the beginning of the transitional zone, with the keystone of the arch in or near the superficial zone where the fiber runs tangential to the cartilage surface before starting its return journey back to the subchondral bone, forming the second pillar of the arch [46]. If we assume the arching parts to be semi-circular, the thickness of the middle zone is theoretically given by the radius of the arches. The constant thickness of the superficial and middle layers and the increasing thickness of the deep layer with increasing total cartilage thickness suggest that the radius of the arches remains constant with their pillars becoming longer. That would mean that the adaptation of the collagen architecture to scaling would consist of the arches becoming more slender with increasing cartilage thickness; and not proportionally increase in size. In this case, the relative number of arches per unit of (subchondral bone plate) surface would remain constant and, given the constant ratio of total collagen to total mass of cartilage, the ratio of collagen fibril thickness to total cartilage thickness would not increase isometrically with the pillars of the arches becoming relatively thinner. However, verification of this theory would require large numbers of samples from differently sized animals from the same species, as there are relatively large differences in configuration of the collagen arches over the species [15].

Interestingly, the response of the subchondral unit seems to be independent of increasing body mass. Although it was hypothesized that the subchondral bone plate thickness would scale with body mass as well, this was not the case. The subchondral bone volume fraction (and subsequently porosity) showed no correlation with BM. This is unexpected, because if the porosity of the interface between cartilage and bone increases in larger animals, this could be explained by the need of

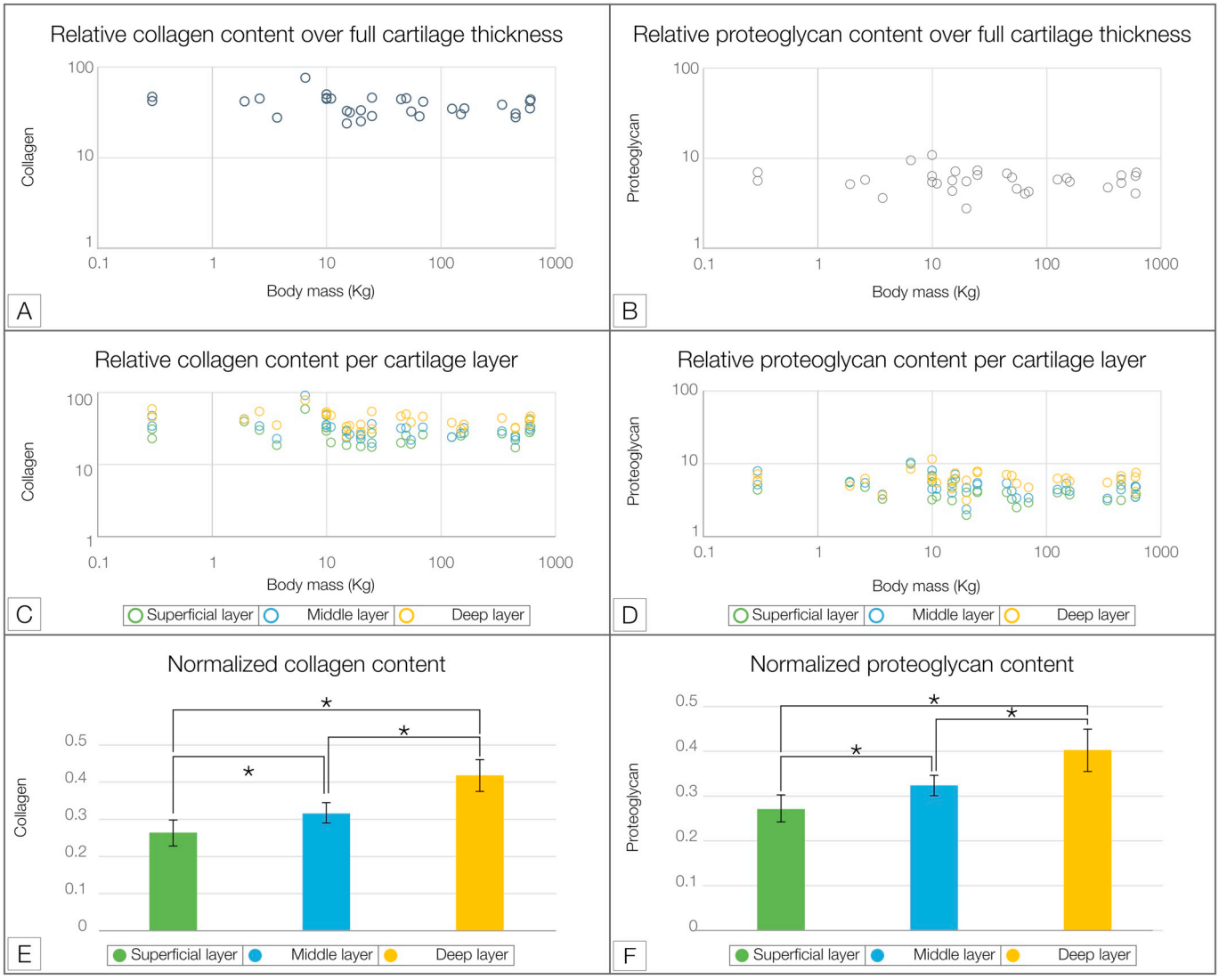

Fig. 5. Relative collagen and proteoglycan contents in cartilage, measured over total thickness (A,B respectively), and layer per layer (C–D). Overall collagen and proteoglycan contents showed no dependency to body mass (collagen, B proteoglycans), with a small variation in cartilage composition across all species. Layer per layer analysis (superficial, middle and deep, respectively in green, blue and yellow) showed this was also true for both collagen and proteoglycans within each specific layer across species (C, D). Normalizing the content of collagen and proteoglycans to total thickness content, deep layer content was highest, and superficial layer was lowest for both collagen and proteoglycans (E, F), and showed significant differences between layers ($*p < 0.05$). (For interpretation of the references to colour in this figure legend, the reader is referred to the web version of this article.)

a less dense structure that could be more able to effectively distribute and transmit forces homogeneously to the underlying trabecular bone [47].

The trabecular bone itself features absolute thicker trabeculae and is denser with increasing body mass to accommodate the higher forces. This could permit accommodation of higher forces and be interpreted as an adaptation to increased body mass. A relatively less dense structure could also allow better nutrition efficiency towards the cartilage by facilitating diffusion from the subchondral bone. However, this should be confirmed by an analysis of micro- and nano-porosity, which would require imaging with a higher resolution than possible with light microscopy. There is in fact evidence in literature that, in an experimental setting, there is exchange of nutrients at the interface of bone and cartilage, although of minimal order compared to the nutrient exchange with the synovial fluid [48]. In fact, Arkill et al. 2008, reported that areas of direct contact of non-calcified cartilage with the subchondral bone allow for a five-fold solute exchange compared to calcified regions [49]. Furthermore they showed that even calcified cartilage is permeable to small solutes so that the subchondral circulation may indeed have a significant role in nutrition of the deep cartilage layer [49]. However, the absence of this correlation suggests that more complex factors may be at play: a possible determinant could reside in the mutable nature of the interface, which may be more dynamic than initially thought [50]. There is abundant evidence suggesting that bone and cartilage crosstalk, as shown per example by the presence of vascular canals in the interface between subchondral bone and calcified cartilage [51,52]. These characteristics suggest that the interface may be less directly influenced by biomechanical loading, as more complex influences contribute to its microstructural features.

The scaling of the trabecular bone features confirmed our hypothesis of negative allometry, with a slope value ($a = 0.14$) in line with previous studies [9]. Interestingly, this relationship was shown to change to isometry when comparing only primates, as demonstrated by a meta-analysis conducted on over 30 primate species by Ryan et al. [53]. The analysis of the relative thickness of cartilage, subchondral plate and trabeculae (Fig. 7) suggests that size may impose different rules at the extremities of the weight spectrum. The relationship seems to be rather similar amongst most species and sizes, but very small and

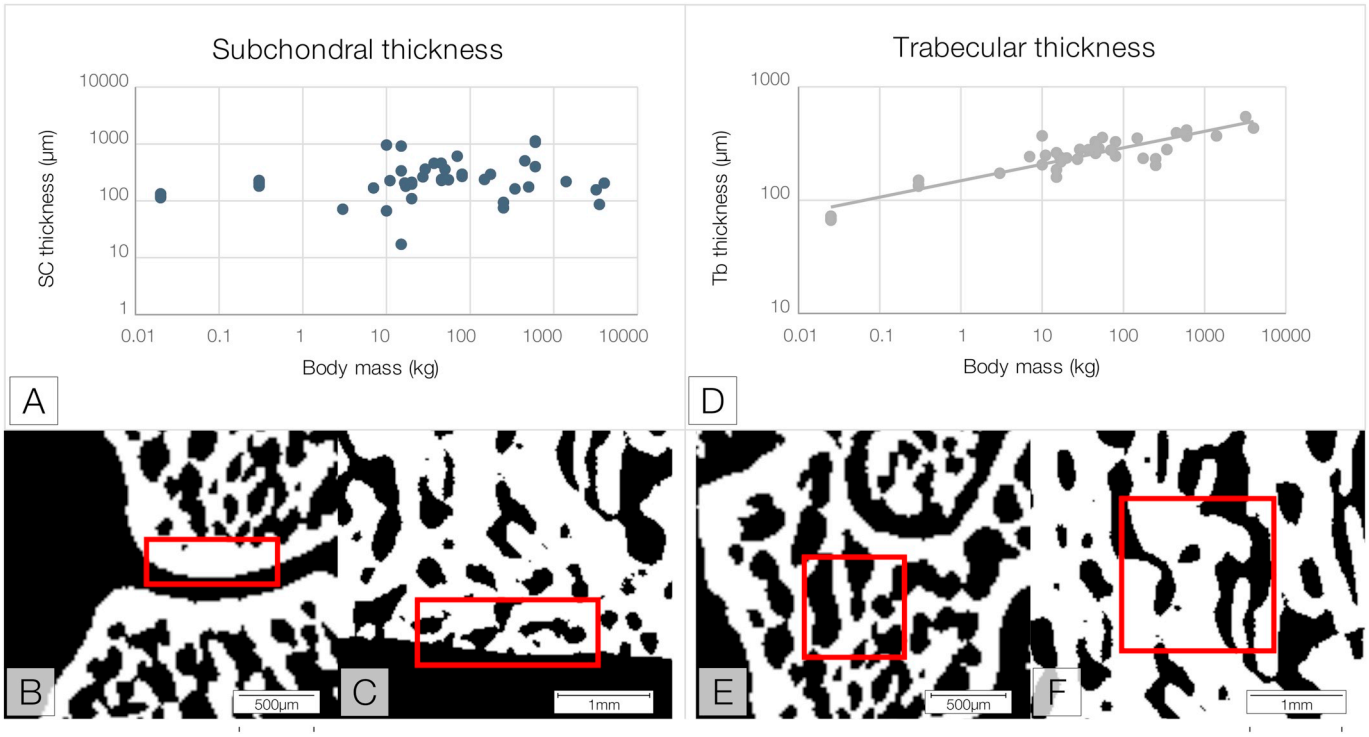

Fig. 6. Scaling of subchondral plate and trabecular thickness. Subchondral plate thickness (Sc Th) showed no correlation to body mass (A). Images obtained with micro-CT of rat (B) and elephant (C) show small differences in subchondral plate (red square) thickness between animals of very different sizes. Trabecular thickness (Tb.Th) correlated to body mass (BM), with a negative allometric relationship to body mass ($r = 0.72$, $a = 0.14$), D). Images obtained with micro-CT rat (E) and elephant (F) show increase in trabecular bone (red square) thickness along BM. (For interpretation of the references to colour in this figure legend, the reader is referred to the web version of this article.)

very large animals appear to have their own ratios when it comes to scaling. Some of these exceptions have been reported in literature, mostly with respect to the smaller species such as mice and rats in which trabecular bone features [9] and cartilage cellularity [7] were shown not to follow the general patterns. Data on the other end of the spectrum are virtually lacking. A much higher sample pool would be needed for statistical confirmation of these trends.

While offering new insights into the variation in the osteochondral unit structure across species, this study has some limitations. Traditional biochemistry still remains the gold standard for the characterization of extracellular matrix composition, but was replaced by FTIRI analysis in this study. This was done because traditional biochemical analysis of the different cartilage layers would have been very difficult and subject to various sources of error [24]. The use of FTIRI has previously been applied for spatial analysis of the main ECM components of cartilage (*i.e.* collagen and proteoglycans) [21–23], but

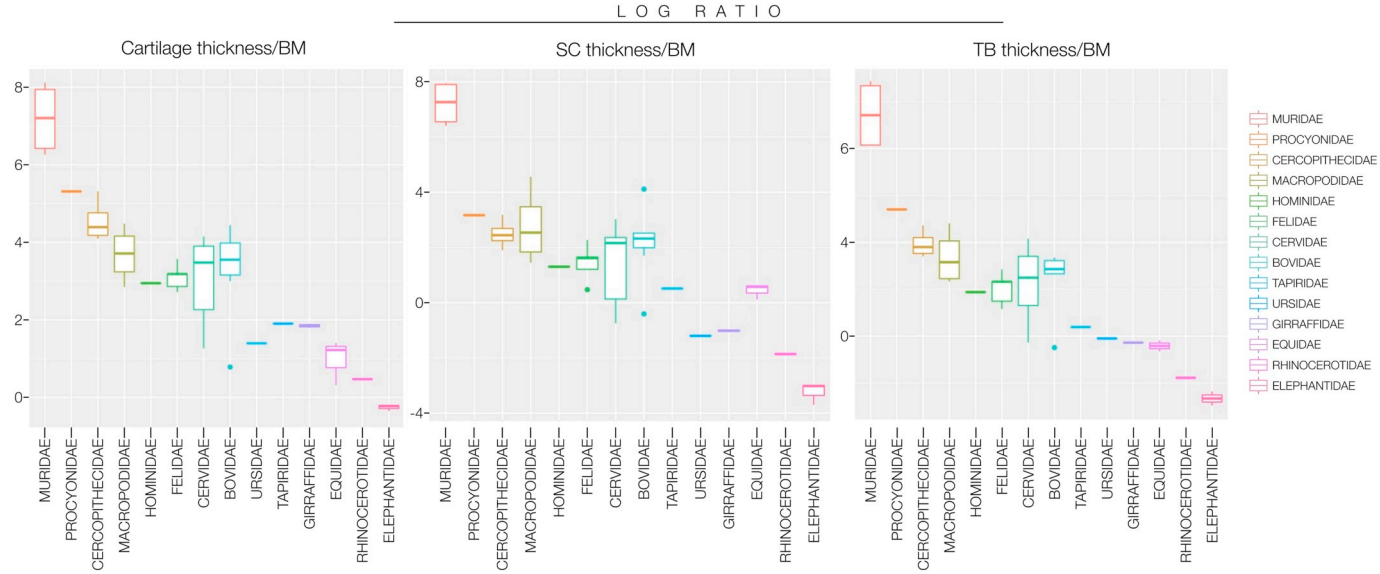

Fig. 7. Analysis of the log ratios of cartilage, subchondral plate and trabecular bone thicknesses, was performed to visualize possible differences between animals at the extremities of BM range (*i.e.* belonging to the Muridae family and to the Elephantidae family), however statistical analysis could not highlight any significant differences.

is performed under controlled atmospheric conditions, in absence of water and on dehydrated sections [21]. This may affect thickness measurements due to shrinkage of samples related to fixation for paraffin embedding; however, it should be noted that the order of shrinkage is largely dependent on water content [54], and is common to all morphological studies performed using fixated tissue. Further, the distribution of components should remain relatively unaltered [55] and in the current study the overall biochemical composition of cartilage was found to be similar to earlier reports using classic biochemical analysis methods [7].

Lastly, standard osteochondral units of 6 mm diameter were harvested and analyzed in all species. These were taken from a weight bearing area of the medial condyle of the femur. In the mouse this means that the sample consisted of virtually the entire condyle, while in the elephant it represented a small portion on the articular surface of the medial condyle. Since it is known that there is topographical heterogeneity in cartilage composition related to weight-bearing [38,56], this means that in the larger species variability may be a little larger depending on exact sample location. However, this effect was most likely limited, as samples were in all cases taken from a load-bearing area. Finally, because samples were harvested from deceased animals brought for necroscopy at Utrecht University, sample size was very limited for some species.

5. Conclusions

Articular cartilage is a tissue with a high degree of specialization that, in a functional sense, can only be appreciated in the wider context of the osteochondral unit. Our findings suggest that the tissue's structure has remained remarkably preserved across mammalian species during evolution, and that the trabecular and subchondral bone -in particular- adapt to the increasing body mass. The natural constancy and apparent immutability of the cartilage should be considered when designing strategies for regeneration and/or functional repair.

Supplementary data to this article can be found online at https://doi.org/10.1016/j.bone.2019.07.001.

Declaration of Competing Interest

Irina A.D. Mancini, Lassi Rieppo, Behdad Pouran, Isaac O. Afara, Filipe M. Serra Braganca, Mattie H.P. van Rijen, Marja Kik, Harrie Weinans, Juha Toyras, René van Weeren and Jos Malda declare that they have no conflict of interest.

Acknowledgements

The authors would like to thank: Chris Van de Lest for the statistical consultancy, Virpi Tiitu for the PLM contribution, Miguel Castilho for the discussion, and VariaVision –Science Division for the figures consultancy. The research leading to these results has received funding from the European Commission Seventh Framework Programme (FP7/2007–2013) under grant agreement 309962 (HydroZONES) and the Dutch Arthritis Foundation (LLP-12 and LLP-22).

References

[1] G. Galilei, Discorsi e dimostrazioni matematiche intorno a due nuove scienze attenenti alla meccanica e i movimenti locali, Ludovico Elzeviri, Leiden, The Netherlands, 1638.
[2] D.H. Allen, How mechanics shaped the modern world, Springer2014.
[3] A.A. Biewener, Scaling body support in mammals: limb posture and muscle mechanics, Science 245 (4913) (1989) 45–48.
[4] M.T. Carrano, Implications of limb bone scaling, curvature and eccentricity in mammals and non-avian dinosaurs, J. Zool. 254 (1) (2001) 41–55.
[5] W.H. Simon, Scale effects in animal joints. I. Articular cartilage thickness and compressive stress, Arthritis & Rheumatism: Official Journal of the American College of Rheumatology 13(3) (1970) 244–255.
[6] A.A. Biewener, Biomechanical consequences of scaling, J. Exp. Biol. 208 (9) (2005) 1665–1676.
[7] J. Malda, J.C. de Grauw, K.E. Benders, M.J. Kik, C.H. van de Lest, L.B. Creemers, W.J. Dhert, P.R. van Weeren, Of mice, men and elephants: the relation between articular cartilage thickness and body mass, PLoS One 8 (2) (2013) e57683.
[8] M. Doube, M.M. Kłosowski, A.M. Wiktorowicz-Conroy, J.R. Hutchinson, S.J. Shefelbine, Trabecular bone scales allometrically in mammals and birds, Proceedings of the Royal Society of London B: Biological Sciences (2011) rspb20110069.
[9] M.M. Barak, D.E. Lieberman, J.-J. Hublin, Of mice, rats and men: trabecular bone architecture in mammals scales to body mass with negative allometry, J. Struct. Biol. 183 (2) (2013) 123–131.
[10] A. Chevrier, A.S. Kouao, G. Picard, M.B. Hurtig, M.D. Buschmann, Interspecies comparison of subchondral bone properties important for cartilage repair, J. Orthop. Res. 33 (1) (2015) 63–70.
[11] R.J. Lories, F.P. Luyten, The bone–cartilage unit in osteoarthritis, Nat. Rev. Rheumatol. 7 (1) (2011) 43.
[12] C.E. Kawcak, C.W. McIlwraith, R. Norrdin, R. Park, S. James, The role of subchondral bone in joint disease: a review, Equine Vet. J. 33 (2) (2001) 120–126.
[13] E. Hunziker, Articular cartilage repair: basic science and clinical progress, A review of the current status and prospects, Osteoarthritis and cartilage 10 (6) (2002) 432–463.
[14] F. Guilak, Biomechanical factors in osteoarthritis, Best Pract. Res. Clin. Rheumatol. 25 (6) (2011) 815–823.
[15] M. Kääb, I. Ap Gwynn, H. Nötzli, Collagen fibre arrangement in the tibial plateau articular cartilage of man and other mammalian species, The Journal of Anatomy 193 (1) (1998) 23–34.
[16] D. Frisbie, M. Cross, C. McIlwraith, A comparative study of articular cartilage thickness in the stifle of animal species used in human pre-clinical studies compared to articular cartilage thickness in the human knee, Vet. Comp. Orthop. Traumatol. 19 (03) (2006) 142–146.
[17] K.D. Jürgens, H. Bartels, R. Bartels, Blood oxygen transport and organ weights of small bats and small non-flying mammals, Respir. Physiol. 45 (3) (1981) 243–260.
[18] R. Froese, Cube law, condition factor and weight–length relationships: history, meta-analysis and recommendations, J. Appl. Ichthyol. 22 (4) (2006) 241–253.
[19] T.J. Klein, J. Malda, R.L. Sah, D.W. Hutmacher, Tissue engineering of articular cartilage with biomimetic zones, Tissue Eng. B Rev. 15 (2) (2009) 143–157.
[20] J. Currey, The many adaptations of bone, J. Biomech. 36 (10) (2003) 1487–1495.
[21] N.P. Camacho, P. West, P.A. Torzilli, R. Mendelsohn, FTIR microscopic imaging of collagen and proteoglycan in bovine cartilage, Biopolymers 62 (1) (2001) 1–8.
[22] A. Boskey, N.P. Camacho, FT-IR imaging of native and tissue-engineered bone and cartilage, Biomaterials 28 (15) (2007) 2465–2478.
[23] K. Potter, L.H. Kidder, I.W. Levin, E.N. Lewis, R.G. Spencer, Imaging of collagen and proteoglycan in cartilage sections using Fourier transform infrared spectral imaging, Arthritis & Rheumatology 44 (4) (2001) 846–855.
[24] L. Rieppo, S. Saarakkala, T. Närhi, J. Holopainen, M. Lammi, H. Helminen, J. Jurvelin, J. Rieppo, Quantitative analysis of spatial proteoglycan content in articular cartilage with Fourier transform infrared imaging spectroscopy: critical evaluation of analysis methods and specificity of the parameters, Microsc. Res. Tech. 73 (5) (2010) 503–512.
[25] A. Changoor, N. Tran-Khanh, S. Methot, M. Garon, M. Hurtig, M. Shive, M. Buschmann, A polarized light microscopy method for accurate and reliable grading of collagen organization in cartilage repair, Osteoarthr. Cartil. 19 (1) (2011) 126–135.
[26] Y. Yarker, R. Aspden, D. Hukins, Birefringence of articular cartilage and the distribution of collagen fibril orientations, Connect. Tissue Res. 11 (2–3) (1983) 207–213.
[27] D.P. Speer, L. Dahners, The collagenous architecture of articular cartilage. Correlation of scanning electron microscopy and polarized light microscopy observations, Clinical orthopaedics and related research (139) (1979) 267–275.
[28] R. Fajardo, R. Müller, Three-dimensional analysis of nonhuman primate trabecular architecture using micro-computed tomography, Am. J. Phys. Anthropol. 115 (4) (2001) 327–336.
[29] D.W. Holdsworth, M.M. Thornton, Micro-CT in small animal and specimen imaging, Trends Biotechnol. 20 (8) (2002) S34–S39.
[30] J. Rieppo, J. Hallikainen, J.S. Jurvelin, I. Kiviranta, H.J. Helminen, M.M. Hyttinen, Practical considerations in the use of polarized light microscopy in the analysis of the collagen network in articular cartilage, Microsc. Res. Tech. 71 (4) (2008) 279–287.
[31] P. Julkunen, P. Kiviranta, W. Wilson, J.S. Jurvelin, R.K. Korhonen, Characterization of articular cartilage by combining microscopic analysis with a fibril-reinforced finite-element model, J. Biomech. 40 (8) (2007) 1862–1870.
[32] J. Arokoski, M.M. Hyttinen, T. Lapveteläinen, P. Takács, B. Kosztáczky, L. Módis, V. Kovanen, H. Helminen, Decreased birefringence of the superficial zone collagen network in the canine knee (stifle) articular cartilage after long distance running training, detected by quantitative polarised light microscopy, Ann. Rheum. Dis. 55 (4) (1996) 253.
[33] M. Doube, M.M. Kłosowski, I. Arganda-Carreras, F.P. Cordelières, R.P. Dougherty, J.S. Jackson, B. Schmid, J.R. Hutchinson, S.J. Shefelbine, BoneJ: free and extensible bone image analysis in ImageJ, Bone 47 (6) (2010) 1076–1079.
[34] R.C. Team, R: A language and environment for statistical computing, R Foundation for Statistical Computing, Vienna, Austria., 2018.
[35] P.C. Brian, G. Peterson, Performance Analytics: Econometric Tools for Performance and Risk Analysis, (2018).
[36] H. Wickham, ggplot2: Elegant Graphics for Data Analysis., Springer-Verlag, New York, 2016.
[37] V.C. Mow, A. Ratcliffe, A.R. Poole, Cartilage and diarthrodial joints as paradigms

for hierarchical materials and structures, Biomaterials 13 (2) (1992) 67–97.
[38] P. Brama, J. Tekoppele, R. Bank, D. Karssenberg, A. Barneveld, P. Weeren, Topographical mapping of biochemical properties of articular cartilage in the equine fetlock joint, Equine Vet. J. 32 (1) (2000) 19–26.
[39] P. Kumar, M. Oka, J. Toguchida, M. Kobayashi, E. Uchida, T. Nakamura, K. Tanaka, Role of uppermost superficial surface layer of articular cartilage in the lubrication mechanism of joints, The Journal of Anatomy 199 (3) (2001) 241–250.
[40] A.J. Sophia Fox, A. Bedi, S.A. Rodeo, The basic science of articular cartilage: structure, composition, and function, Sports health 1 (6) (2009) 461–468.
[41] H. Muir, P. Bullough, A. Maroudas, The distribution of collagen in human articular cartilage with some of its physiological implications, The Journal of bone and joint surgery. British volume 52 (3) (1970) 554–563.
[42] S. Bevill, A. Thambyah, N. Broom, New insights into the role of the superficial tangential zone in influencing the microstructural response of articular cartilage to compression, Osteoarthr. Cartil. 18 (10) (2010) 1310–1318.
[43] R. Korhonen, M. Wong, J. Arokoski, R. Lindgren, H. Helminen, E. Hunziker, J. Jurvelin, Importance of the superficial tissue layer for the indentation stiffness of articular cartilage, Med. Eng. Phys. 24 (2) (2002) 99–108.
[44] M.A. Peterson, Galileo's discovery of scaling laws, Am. J. Phys. 70 (6) (2002) 575–580.
[45] J. Malda, K. Benders, T. Klein, J. De Grauw, M. Kik, D. Hutmacher, D. Saris, P. Van Weeren, W. Dhert, Comparative study of depth-dependent characteristics of equine and human osteochondral tissue from the medial and lateral femoral condyles, Osteoarthr. Cartil. 20 (10) (2012) 1147–1151.
[46] A. Benninghoff, Form und Bau der Gelenkknorpel in ihren Beziehungen zur Funktion, Z. Zellforsch. Mikrosk. Anat. 2 (5) (1925) 783–862.
[47] K. Pałka, R. Pokrowiecki, Porous Titanium Implants: A Review, Advanced Engineering Materials (2018).
[48] B. Pouran, V. Arbabi, R.L. Bleys, P.R. van Weeren, A.A. Zadpoor, H. Weinans, Solute transport at the interface of cartilage and subchondral bone plate: effect of micro-architecture, J. Biomech. 52 (2017) 148–154.
[49] K. Arkill, C. Winlove, Solute transport in the deep and calcified zones of articular cartilage, Osteoarthr. Cartil. 16 (6) (2008) 708–714.
[50] D.M. Findlay, J.S. Kuliwaba, Bone–cartilage crosstalk: a conversation for understanding osteoarthritis, Bone research 4 (2016) 16028.
[51] J. Clark, J. Huber, The structure of the human subchondral plate, The Journal of bone and joint surgery. British volume 72 (5) (1990) 866–873.
[52] H. Imhof, I. Sulzbacher, S. Grampp, C. Czerny, S. Youssefzadeh, F. Kainberger, Subchondral bone and cartilage disease: a rediscovered functional unit, Investig. Radiol. 35 (10) (2000) 581–588.
[53] T.M. Ryan, C.N. Shaw, Trabecular bone microstructure scales allometrically in the primate humerus and femur, Proc. R. Soc. Lond. B Biol. Sci. 280 (1758) (2013) 20130172.
[54] E.B. Hunziker, K. Lippuner, N. Shintani, How best to preserve and reveal the structural intricacies of cartilaginous tissue, Matrix Biol. 39 (2014) 33–43.
[55] J. Kiviranta, M. Tammi, J. Jurvelin, A.-M. Säämänen, H. Helminen, Fixation, decalcification, and tissue processing effects on articular cartilage proteoglycans, Histochemistry 80 (6) (1984) 569–573.
[56] I. Kiviranta, J. Jurvelin, M. Tammi, A.M. SääMäunen, H.J. Helminen, Weight bearing controls glycosaminoglycan concentration and articular cartilage thickness in the knee joints of young beagle dogs, Arthritis & Rheumatology 30 (7) (1987) 801–809.